CORRECTED 13 MAY 2015; SEE ERRATUM

RESEARCH ARTICLE

BIOENGINEERING

Mitigation of tracheobronchomalacia with 3D-printed personalized medical devices in pediatric patients

Robert J. Morrison,[1] Scott J. Hollister,[2] Matthew F. Niedner,[3] Maryam Ghadimi Mahani,[4] Albert H. Park,[5] Deepak K. Mehta,[6] Richard G. Ohye,[7] Glenn E. Green[8]*

Three-dimensional (3D) printing offers the potential for rapid customization of medical devices. The advent of 3D-printable biomaterials has created the potential for device control in the fourth dimension: 3D-printed objects that exhibit a designed shape change under tissue growth and resorption conditions over time. Tracheobronchomalacia (TBM) is a condition of excessive collapse of the airways during respiration that can lead to life-threatening cardiopulmonary arrests. We demonstrate the successful application of 3D printing technology to produce a personalized medical device for treatment of TBM, designed to accommodate airway growth while preventing external compression over a predetermined time period before bioresorption. We implanted patient-specific 3D-printed external airway splints in three infants with severe TBM. At the time of publication, these infants no longer exhibited life-threatening airway disease and had demonstrated resolution of both pulmonary and extrapulmonary complications of their TBM. Long-term data show continued growth of the primary airways. This process has broad application for medical manufacturing of patient-specific 3D-printed devices that adjust to tissue growth through designed mechanical and degradation behaviors over time.

INTRODUCTION

Three-dimensional (3D) printing or additive manufacturing arose from the automotive and aerospace industry in the 1980s and has subsequently been applied to customization of medical devices (*1*). In health care, 3D printing was initially applied for manufacturing of hearing aids, amputee prosthetics, and wearable dental appliances (*2*). Medical uses to date have been confined to static structures, including patient-specific craniofacial implants for reconstruction of the skull and facial skeleton, titanium hip and mandibular prostheses, and scaffolding for tissue engineering (*1*, *3*, *4*). Producing 3D-printed devices that adapt to growing or changing tissues is important for pediatric applications. Static preclinical 3D-printed scaffolds have been investigated for tracheal tissue engineering (*5*); however, to our knowledge, 3D printing has not been adapted for treating pediatric airway disorders. 3D printing has currently untapped potential to provide custom, protean devices for challenging and life-threatening disease processes.

Selected 3D-printable biomaterials have created the potential for 4D structure. These 3D-printed objects exhibit engineered shape change owing to design-influenced mechanical and degradation deformation in response to tissue growth over a defined time period (*6*). Pediatric deformities would, in particular, benefit from "4D materials" and the ability to change with growth. Pediatric tracheobronchomalacia (TBM) is a condition of excessive collapse of the airways during respiration that can lead to life-threatening cardiopulmonary arrests (*7*, *8*). As children grow, the airway cartilage strengthens, and disease severity commonly regresses; however, infants with severe disease require aggressive therapy and are at imminent risk of death from refractory respiratory failure and complicated pulmonary infections (*9*). Current standard therapies include tracheostomy tube placement with prolonged mechanical ventilation, cardiovascular procedures to relieve compression from abnormal anatomy, and intraluminal airway stents. However, all treatment options have high complication and failure rates.

Annual incidence of respiratory arrest owing to tube occlusion after pediatric tracheostomy is as high as 43% (*10*, *11*). Additionally, pediatric tracheostomy with prolonged mechanical ventilation is associated with developmental delay and secondary airway stenosis that frequently requires operative correction (*12*). Surgical correction of secondary lesions causing TBM, such as aortopexy and tracheoplasty, carries a complication rate of 36%, including pericardial effusion, mediastinitis, and recurrence or regression of disease with cardiopulmonary arrest (*9*, *13*). Tracheal stenting can result in recurrence of airway obstruction due to granulation tissue formation or stent migration in 43% of cases, and cardiopulmonary arrest and death have been described (*13*). There is a specific U.S. Food and Drug Administration (FDA) warning against the use of airway stents in children (*14*). Currently, the most severe forms of TBM lack an adequate intervention (*9*, *13*).

If a child can be supported through the first 24 to 36 months of TBM, airway growth generally results in a natural resolution of this disease. Typically, human anatomic structures obey the square-cube law with growth, where volume of structures increases at a faster rate than area, with adults often scaling to 10 to 20 times the volumetric size of neonates. Airway stents and prosthetics frequently fail because of inability to accommodate airway growth. Fixed-size external implants may restrict airway growth and inhibit natural improvement of the disease past the critical period (*15*). Fixed-size intraluminal devices are prone to migration and can require frequent procedures to resize the device. Intraluminal devices are prone to mucous plugging owing to the small caliber of the pediatric airway and disruption of the natural mucociliary clearance mechanism, with resultant cardiopulmonary arrest.

Our multidisciplinary team designed an archetype device to allow radial expansion of the affected airway over the critical growth period

[1]Department of Otolaryngology-Head and Neck Surgery, University of Michigan, Ann Arbor, MI 48109, USA. [2]Department of Biomedical Engineering, University of Michigan, Ann Arbor, MI 48109, USA. [3]Department of Pediatrics, Division of Critical Care Medicine, University of Michigan, Ann Arbor, MI 48109, USA. [4]Department of Radiology, University of Michigan, Ann Arbor, MI 48109, USA. [5]Division of Otolaryngology-Head and Neck Surgery, Department of Surgery, University of Utah, Salt Lake City, UT 84132, USA. [6]Department of Pediatric Otolaryngology, Children's Hospital of Pittsburgh of University of Pittsburgh Medical Center, Pittsburgh, PA 15224, USA. [7]Department of Cardiac Surgery, University of Michigan, Ann Arbor, MI 48109, USA. [8]Department of Otolaryngology-Head and Neck Surgery, Division of Pediatric Otolaryngology, University of Michigan, Ann Arbor, MI 48109, USA.
*Corresponding author. E-mail: gegreen@med.umich.edu

while resisting external compression and intrinsic collapse. Patient-specific devices are designed by image-based computer-aided design (CAD) and manufactured using a 3D printer. In a preclinical porcine model of TBM, the device demonstrated increased survival compared to the untreated group (*16*). Implantation in one neonate with TBM demonstrated early in-human feasibility (*17*). Nevertheless, there are a number of design control, manufacturing, and regulatory considerations that preclude capricious application of 3D-printed medical devices.

Here, we report three pediatric patients with severe TBM successfully treated with a 3D-printed personalized bioresorbable medical device, designed to accommodate airway growth while preventing external compression over a designed time period before bioresorption. We demonstrate the use of this process to treat bilateral disease and the first sustained cure of associated protein-losing enteropathy (PLE). The details of device design and manufacturing, analysis of device efficacy, and the effect of the device on long-term airway growth are reported.

RESULTS

Tracheobronchial splint device design

In creating a device that could be responsive to airway geometry changes with growth as well as the natural history of the condition, we considered the principles of 4D printing: the geometric program, the material, and the machine (*6*). The archetype device design was an open, bellowed cylinder with 10 design variables to allow placement of the splint external to the collapsed airway (Fig. 1A). The walls of the airway were suspended to the framework of the splint via sutures placed through designed suture hole interstices (Fig. 1B). Placement of the splint immediately increased the radius of the airway with a corresponding increase in airflow as characterized by the Hagen-Poiseuille equation. External placement also allowed the splint to aid in protection of the airway from compression. The bellowed topology allowed longitudinal flexion.

Although immediate improvement in airflow is attributable to the external placement of the splint and increase in lumen diameter, sustained benefit was dependent on the ability of the device to be responsive to airway growth. An open cylindrical design was incorporated to allow opening of the device with radial growth of the airway via displacement of the open wedge angle (movie S1). This device geometric program was used to permit conformational change beyond what could be achieved with material choice, allowing accommodation of airway growth beyond what would be possible simply owing to the reduction in device stiffness from material degradation alone. Using images of the airway from the patient's computed tomography (CT) scan, which were imported into a CAD modeling program (Mimics, Materialise), measurements were made to determine the geometric design parameters of the splint (Fig. 1C). Customization of the design parameters to patient anatomy was performed to submillimeter accuracy using this process. Design parameters were used to generate the device design, which was output as a series of 2D images and used to generate the 3D model of the splint (Fig. 1D). Furthermore, the resulting 3D splint design was digitally fit to the patient airway for validation (Fig. 1E).

The splint was manufactured using polycaprolactone (PCL) (Fig. 1F), a biocompatible and bioresorbable polyester that remains in vivo for 2 to 3 years before resorption. We demonstrated previously that PCL does not exhibit molecular weight, molecular number, or polydispersity alteration during 3D printing (*18*). About 200 splints may be fabricated in 4 hours using this manufacturing technique. The devices were ethylene oxide–sterilized before implantation.

The design parameters for the splints for each patient are listed in Table 1. Owing to the presence of bilateral severe mainstem bronchomalacia, the left splint design of patient 2 was modified to incorporate a spiral to the open face of the cylinder, to accommodate the spatial position of the right splint and bronchus (Fig. 1F). This design modification was accomplished in 3 hours and printed the next day, demonstrating the adaptability and precision possible with 3D printing. The time from initial patient candidacy evaluation to production of the device, encompassing imaging, CAD, and 3D laser sinter manufacture, was 2 days for patient 1, 4 days for patient 2, and 5 days for patient 3.

All splint designs met designed virtual mechanical performance criteria when assessed with finite element analysis (fig. S1). All manufactured splints met mechanical performance criteria (table S1). Justification for selected mechanical performance criteria is based on previous studies of tracheal growth (*16*, *19*–*21*) and are provided in the Supplementary Materials and Methods. From these studies, we predicted that the maximum change in tracheal diameter over the course of 3 years would be 19% (table S2).

Clinical history of three pediatric patients with life-threatening TBM

Patient 1. Patient 1 was a 3-month-old male with life-threatening TBM. At the time of referral, with a customized tracheostomy and high-pressure ventilation [positive end-expiratory pressure (PEEP) of 14 cm H_2O], he required around-the-clock sedation to prevent desaturations to an oxygen saturation (SpO_2) of 10%. Intermittent paralytics were required to maintain ventilation, and intermittent fluid boluses were required to maintain blood pressure. Imaging studies demonstrated complete collapse and persistent narrowing of the left mainstem bronchus with concomitant air trapping and hyperexpansion of the left lung. This defect resulted in an increasingly elevated arterial and venous carbon dioxide partial pressure (pCO_2) of 80.1 mmHg (normal, 41.0 to 51.0 mmHg) and compensatory metabolic alkalosis with an elevated bicarbonate (HCO_3) of 42.2 mM (normal, 22.0 to 26.0 mM) to maintain his low-normal pH (7.34). A postobstructive pulmonary infection was noted. His additional morbidities included crisscross orientation of the left and right pulmonary arteries with hypoplastic right pulmonary artery, abdominal ascites, and abdominal distension of unknown etiology.

Patient 2. Patient 2 was a 16-month-old male with life-threatening TBM. At the time of referral, he has a tracheostomy and required very high-pressure ventilation (PEEP of 20 cm H_2O) with around-the-clock sedation to prevent severe desaturations and bradycardia. He intermittently required paralytics and induced comas to maintain ventilation. He had decompensated with minor viral illnesses (rhinovirus and rotavirus) requiring prolonged intensive care unit care. He had been unable to be discharged home since birth and had development digression. Imaging studies and prior diagnostic laryngoscopy and bronchoscopy showed bilateral severe focal mainstem bronchomalacia with complete collapse of the left mainstem bronchus and concomitant air trapping and hyperexpansion of the left lung. The etiology of bronchomalacia was largely attributed to a dilated pulmonary arterial system due to the patient's tetralogy of Fallot leading to compression of the mainstem bronchi. This defect resulted in recurrent postobstructive pulmonary infections including *Klebsiella*, *Pseudomonas*, and *Achromobacter* organisms. Additional problems include partial DiGeorge syndrome and repaired tetralogy of Fallot with absent pulmonary valve and diminutive

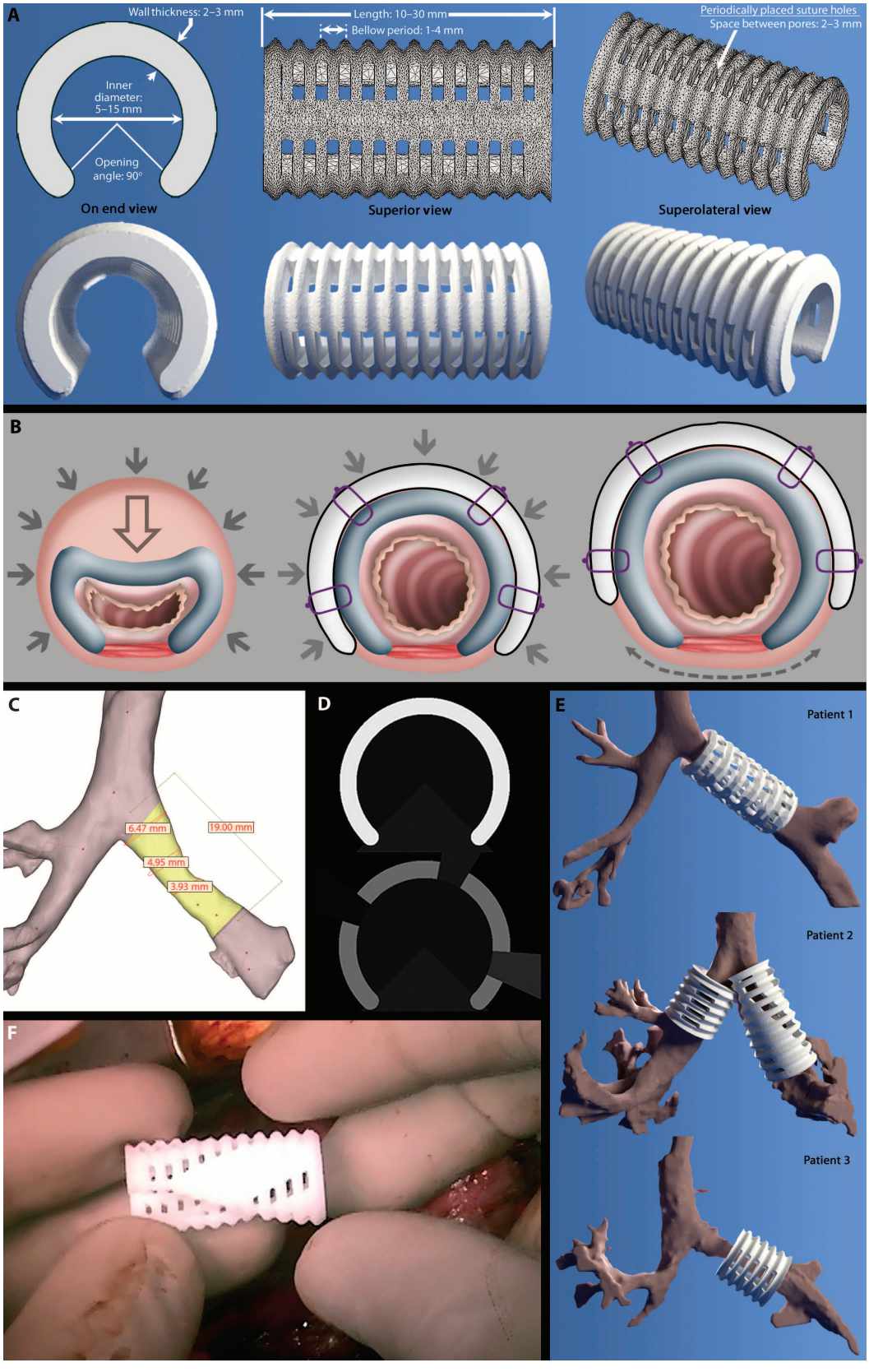

Fig. 1. Computational image-based design of 3D-printed tracheobronchial splints. (**A**) Stereolithography (.STL) representation (top) and virtual rendering (bottom) of the tracheobronchial splint demonstrating the bounded design parameters of the device. We used a fixed open angle of 90° to allow placement of the device over the airway. Inner diameter, length, wall thickness, and number and spacing of suture holes were adjusted according to patient anatomy (Table 1) and can be adjusted on the submillimeter scale. Bellow height and periodicity (ribbing) can be adjusted to allow additional flexion of the device in the *z* axis. (**B**) Mechanism of action of the tracheobronchial splint in treating tracheobronchial collapse in TBM. Solid arrows denote positive intrathoracic pressure generated on expiration. Hollow arrow denotes vector of tracheobronchial collapse. Dashed arrow denotes vector of opening wedge displacement of the tracheobronchial splint with airway growth. (**C**) Digital Imaging and Communications in Medicine (DICOM) images of the patient's CT scan were used to generate a 3D model of the patient's airway via segmentation in Mimics. A centerline was fit within the affected segment of the airway, and measurements of airway hydraulic diameter (DH) and length were used as design parameters to generate the device design. (**D**) Design parameters were input into MATLAB to generate an output as a series of 2D. TIFF image slices using Fourier series representation. Light and gray areas indicate structural components; dark areas are voids. The top image demonstrates a device bellow, and the bottom image demonstrates suture holes incorporated into the device design. The .TIFF images were imported into Mimics to generate an. STL of the final splint design. (**E**) Virtual assessment of fit of tracheobronchial splint over segmented primary airway model for all patients. (**F**) Final 3D-printed PCL tracheobronchial splint used to treat the left bronchus of patient 2. The splint incorporated a 90° spiral to the open angle of the device to accommodate concurrent use of a right bronchial splint and growth of the right bronchus.

Table 1. Design parameters for pediatric tracheobronchial splints.

Patient	Side of bronchus	Wall thickness (mm)	Inner diameter (mm)	Bellow period (mm)	Length (mm)	Spiral
1	Left	2	7	2	19	No
2	Right	2	8	2	12	No
	Left	2	7	2	23	Yes
3	Left	2	6.5	2	11.5	No

blood flow through the left pulmonary artery attributed to chronic hyperexpansion of the left lung. His additional morbidities included abdominal distension with gastrostomy tube dependence secondary to PLE, immunodeficiency with hypogammaglobulinemia, recurrent bacterial infections, including vancomycin-resistant *Enterobacter* bacteremia and *Pseudomonas* mediastinitis, and renal tubular acidosis.

Patient 3. Patient 3 was a 5-month-old male with life-threatening TBM. At the time of referral, he had a tracheostomy, was ventilator-dependent, and required around-the-clock intravenous sedation and narcotics to prevent severe desaturations with bradycardia. He had persistent hypercarbia (pCO_2 of 68.9 mmHg) and acidemia (pH of 7.32). He had required prolonged hand-bag ventilation for severe desaturations multiple times per day. He had previously desaturated to an SpO_2 of 7% and required hand-bag ventilation for a continuous 8-hour period the week before his operation. Patient 3 was unable to take nutrition via gastrostomy owing to subsequent severe desaturations requiring manual resuscitation and also suffered from abdominal distension of unclear etiology. Imaging studies and diagnostic laryngoscopy and bronchoscopy showed severe left mainstem bronchomalacia with distal segmental bronchomalacia and complete collapse of the left mainstem bronchus with concomitant air trapping and hyperexpansion of the left lung. He also had moderate distal tracheomalacia and granulation tissue at the site of a previous tracheal stenosis repair. The etiology of bronchomalacia was primarily attributed to a dilated pulmonary arterial system associated with his tetralogy of Fallot leading to left mainstem bronchus compression. His additional morbidities included tetralogy of Fallot with absent pulmonary valve that had previously been repaired, multiple venous thromboses, failure to thrive, *Pseudomonas* mediastinitis, and a congenital right upper extremity disorder.

Marked physiologic improvements in three TBM patients after surgical implantation

After exposure of affected airways via sternotomy, the splint was placed around the affected airway and secured with polypropylene sutures (fig. S2). Examination of the airway immediately after placement of the tracheobronchial splint via flexible bronchoscopy demonstrated patency of the affected segment, confirmed by imaging 1 month postoperatively (Fig. 2).

Patient 1. After splint implantation, blood gases returned to normal and remained normal at 3-month follow-up (table S3). No intra- or postoperative complications were noted. Seven days after placement of the airway splint, weaning from mechanical ventilation was initiated. Three weeks after the procedure, ventilator support was discontinued entirely, and the child was discharged home (Fig. 3A). Repeat laryngoscopy and bronchoscopy were performed 1, 3, 6, 12, and 38 months postoperatively and demonstrated continued resolution of the bronchomalacia (Fig. 2A). Noncontrasted magnetic resonance imaging (MRI) detected the splint in the proper position at 6 and 12 months after implantation (Fig. 2A, lower middle). At 38 months after implantation, focal fragmentation and mechanical degradation of the splint was noted (Fig. 2A, bottom). Patient 1 is now 38 months after implantation of the tracheobronchial splint and continues to do well with no problems related to the device. He remains tracheostomy-dependent owing to proximal cervical tracheomalacia at his tracheostoma. He has had no recurrent symptoms of bronchomalacia since discharge from the hospital.

Patient 2. After placement of the splint, patient 2 experienced doubling of tidal volumes (from 5 to 10 ml/kg), set PEEP was decreased from 20 to 13 cm H_2O, and the left lung perfused (Fig. 3A). There were no intra- or postoperative complications. Given the degree of the patient's opioid and benzodiazepine dependence and the long-standing nature of his ventilator dependence, a controlled wean from the ventilator was instituted. Four weeks after surgery, the patient was transitioned to a portable ventilator system. MRI imaging at 1 month after surgery showed both splints in the proper position, whereas repeat CT imaging showed patent bronchi bilaterally with resolution of left lung air trapping (Fig. 2B). Patient 2 has been discharged home for the first time in his life and is now 14 months removed from implantation of bilateral tracheobronchial splints. Fifteen weeks postoperatively, he was successfully removed from ventilator support while awake. He continues to do well with no problems related to the device.

Immediately after surgery, the patient continued to suffer from protein-losing diarrheal episodes, hypoalbuminemia, and hypogammaglobulinemia, requiring intermittent albumin and intravenous immunoglobulin G (IgG) supplementation consistent with PLE. He underwent upper gastrointestinal endoscopy and colonoscopy, which demonstrated mildly erythematous duodenopathy without evidence of any secondary causes of PLE such as lymphangiectasias, inflammation, granulomas, chronic architectural changes, organisms, or viral inclusions. As ventilatory pressures were weaned, his diarrhea resolved, serum albumin and immunoglobulin levels normalized, and abdominal ascites and anasarca resolved (Fig. 3B). He is no longer functionally immunosuppressed, has experienced no recurrent opportunistic infections, and no longer requires intravenous albumin or immunoglobulin supplementation.

Patient 3. After implantation of the splint, patient 3 experienced cessation of his life-threatening desaturation episodes related to TBM. The patient tolerated conventional mechanical ventilation with a minimal PEEP (5 mm H_2O) (Fig. 3A). Tidal volumes improved to 10 to 12 ml/kg. There were no intra- or postoperative complications. Repeat CT imaging at 1 month after surgery showed continued patency of the left mainstem bronchus with resolution of left lung air trapping (Fig. 2C). Patient 3 is now 11 months removed from implantation, and there have been no complications attributable to implantation of the splint. He remains on continuous ventilatory support presumably because of distal left segmental bronchomalacia beyond what the splint was designed to address.

Improved patency and similar growth to normal airways of splinted airways

Comparison of airway D_H and airway cross-sectional area (A^2) before and 1 month after implantation of the tracheobronchial splint showed a significant increase in D_H and A^2 for all bronchi in all patients (Table 2).

Comparison of airway caliber (D_H and A^2) at 1 and 30 months postoperatively was performed in patient 1, of whom we have the longest postoperative interval, and demonstrated a significant increase in caliber at 30 months postoperatively (Table 2). Additionally, there was no difference between D_H ($P = 0.35$) or A^2 ($P = 0.12$) of the splinted bronchus and the normal, contralateral bronchus 30 months after implantation of the device (Student's *t* test).

A summary of change in airway caliber before and after device implantation is presented in Fig. 4 for all three patients. The splinted bronchus immediately matched with its normal, contralateral bronchus in patients 1 and 3, and both airways grow along the same vector after application of the splint. Comparative analysis of airway growth in patient 2 was not possible because both mainstem bronchi received a tracheobronchial splint.

DISCUSSION

We report successful implantation of 3D-printed, patient-specific bioresorbable airway splints for treatment of severe TBM. The personalized splints conformed to the patients' individual geometries and expanded with airway growth (in the "fourth dimension"). This confirms the device design and that PCL can serve as a "4D biomaterial" with both shape and material changes over time. In no case was any adverse reaction or complication attributable to the tracheobronchial splint. The three pediatric patients implanted with these 3D-printed airway splints had a terminal form of TBM. The clinical improvement in each case was immediate and sustained, suggesting that improvement is not attributable to natural history of the disease alone.

To design a device using a 4D biomaterial, we planned for degradation and expansion of the device concurrent with growth of the tracheobronchial tree over time. Although there are no published data on biomechanical properties of the pediatric trachea or bronchus, previous work has found that pig tracheas deformed 50% under an applied compressive load of 20 N with a maximum force in bending of 0.3 N (1.5% compression) (*20*). Thus, we defined our maximum compressive allowance as less than 50% deformation under a 20-N load. However, a similar degree of bending compliance was too low for the splint to be effective at maintaining airway patency. We expected that under a 20-N load, the splint should allow greater than 20% displacement in bending to accommodate flexion of the airway but less than 50% displacement (greater than which may interrupt airflow).

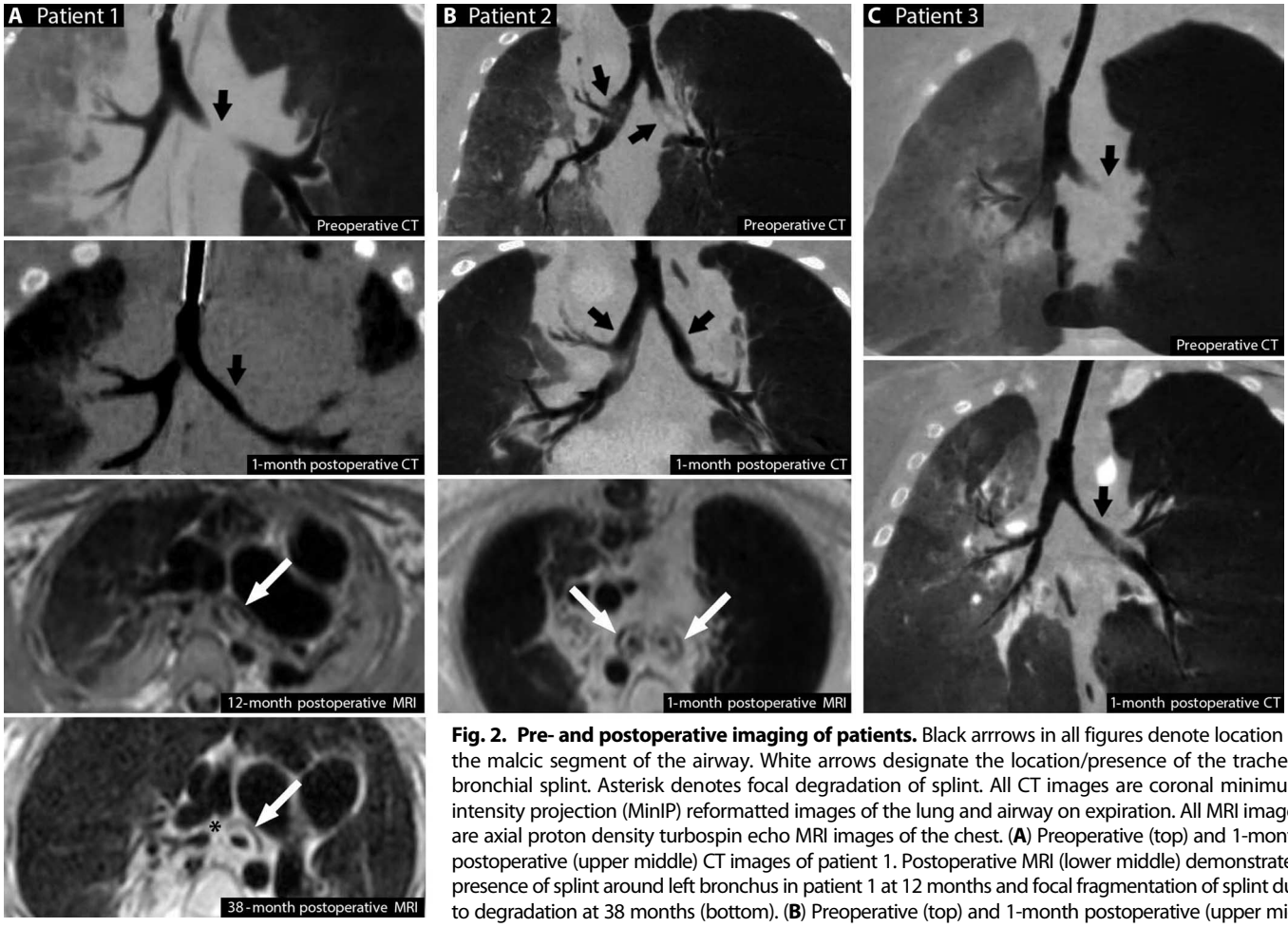

Fig. 2. Pre- and postoperative imaging of patients. Black arrrows in all figures denote location of the malcic segment of the airway. White arrows designate the location/presence of the tracheobronchial splint. Asterisk denotes focal degradation of splint. All CT images are coronal minimum intensity projection (MinIP) reformatted images of the lung and airway on expiration. All MRI images are axial proton density turbospin echo MRI images of the chest. (**A**) Preoperative (top) and 1-month postoperative (upper middle) CT images of patient 1. Postoperative MRI (lower middle) demonstrated presence of splint around left bronchus in patient 1 at 12 months and focal fragmentation of splint due to degradation at 38 months (bottom). (**B**) Preoperative (top) and 1-month postoperative (upper middle) CT images of patient 2. Postoperative MRI (lower middle) demonstrated presence of splints around the left and right bronchi in patient 2 at 1 month. Note that the patient had bilateral mainstem bronchomalacia and received a tracheobronchial splint on both the left and right mainstem bronchus. (**C**) Preoperative (top) and 1-month postoperative (bottom) CT images of patient 3.

Growth data for the mainstem bronchus are not presently available in the literature. The best data available on tracheal growth were provided in adolescent patients with both normal tracheas and tracheostomies (*19*), which provided an equation for calculating narrowest tracheal diameter by age. We applied these equations to the extreme age ranges (3 months to 15 years) of potential patients and predicted that the maximum diameter expansion of the trachea over 3 years would be 19%. However, the pressure exerted by the human growing trachea is unknown. Banding of a rat trachea with a plastic restricted radial expansion by about 50% (*21*); thus, we defined that the splint should allow a 20% expansion of tracheobronchial diameter under minimal expansion pressure. We defined minimal expansion pressure as the pressure exerted by the aorta in systole, based on the assumption that if the pressure exerted by tracheobronchial growth does not at least equal the maximum compression pressure of the aorta, radial growth of the airway would not be observed. Assuming aortic systolic pressure less than 250 mmHg (or 0.03 MPa) and a splint surface area of 400 mm^2, we defined our maximum opening displacement parameter as any pressure greater than 15 N, allowing at least 20% diameter expansion of the splint. Our results confirm that a device that fulfills these mechanical criteria performs as required clinically.

We have previously demonstrated that laser-sintered PCL constructs undergo slow molecular weight loss without substantial shape alteration for the first 18 months when implanted into the cervical intervertebral disc space of large preclinical porcine models (*18*). These results were consistent with bulk hydrolytic degradation processes. Previous work has demonstrated that PCL rods undergo nonlinear molecular weight loss for 24 months, fragment into low–molecular weight pieces from 24 to 36 months, subsequently metabolize, and are excreted completely in urine and feces in a rat model (*22*). For patient 1, MRI and

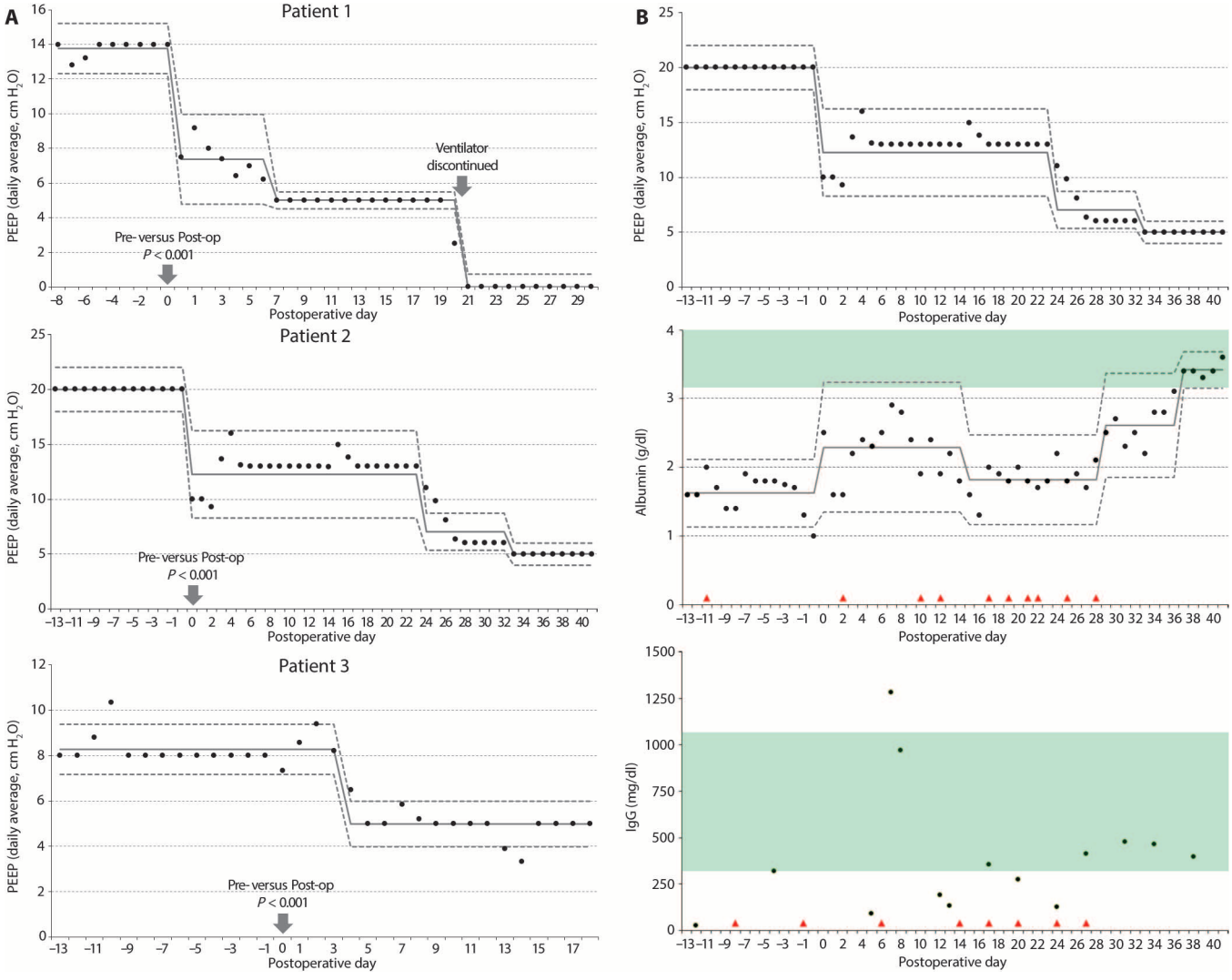

Fig. 3. PEEP, albumin, and immunoglobulin levels of patients after splint. Time 0 on the *x* axis of all graphs is the day of tracheobronchial splint implantation. (**A**) Control charts of PEEP ventilatory requirements for patients 1 to 3 over time. Solid line denotes the steady-state mean, and dashed lines denote upper and lower control limits. Comparison of pre- (Pre-) and postoperative (Post-op) PEEP requirements was performed using a Wilcoxon signed-rank test ($\alpha = 0.05$, two-sided). (**B**) Control chart of PEEP ventilatory requirement, control chart of serum albumin measurement, and run chart of serum IgG measurement over time for patient 2. Solid lines denote the steady-state mean, and dashed lines denote upper and lower control limits. Red arrows denote days intravenous albumin or intravenous IgG was administered. Shaded areas denote normal range of values for albumin (middle) and IgG (bottom).

endoscopy at 38 months demonstrated focal degradation of the splint and dynamic bronchial wall movement, consistent with bioresorption. PCL thus appears to be an ideal substrate for a bioresorbable device whose degradation profile matches the natural time course of disease improvement in pediatric TBM.

Our data suggest that early treatment of TBM may circumvent complications of conventional treatment, such as tracheostomy, prolonged hospitalization and mechanical ventilation, cardiopulmonary arrest, discomfort, and other sequelae. However, this report was not designed for definitive testing of device safety, and rare potential complications of this therapy may not yet be evident. Further patient accruement and analysis under an FDA-enabled clinical trial will be necessary. Only patient 1 has had a sufficient postoperative interval to assess long-term airway growth. The remaining patients are being closely monitored. The use of a noninterventional control group was not ethical, given the severity of the disease treated.

The potential applications of 3D printing in medicine span from customized prosthetics to patient-specific drugs to organogenesis (*3*, *23*–*30*). This study advances the field of 3D printing by integrating patient-specific, image-based design with a biomaterial structure to produce biomechanical behaviors over a designated time period, including expansion over time to accommodate airway growth. Some standard airway implants may be manually modified by their surgeon to match a patient's anatomy (*31*–*33*). In contrast, these 3D-printed implants are directly engineered to the patient's anatomy at a submillimeter resolution. This degree of patient specificity and precision is beyond what is available with standard manufactured devices.

Additionally, 3D-printed devices are scalable to mass-manufacturing levels, which is not currently possible with tissue-engineered tracheal solutions. In our study, each device was designed using patient anatomy to generate device parameters—a design process that is consistent with the philosophy of personalized medicine. The devices were designed to meet mechanical performance criteria that were unattainable by material degradation alone, including allowing greater than 20% expansion of the airway diameter under minimal airway growth

Table 2. Airway caliber measurements before and after implantation in three pediatric patients. All measurements were made on expiratory scans using the centerline function of each isolated treated or contralateral normal mainstem bronchus in Mimics. (**A** and **B**) The centerline function measures D_H (A) and A^2 (B) every 0.1 to 1.0 mm along the entire segment of the isolated model (in this case, the mainstem bronchus). Data are means ± SD. The *n* listed under each mean is the number of measurements performed on each bronchus by the centerline function.

Time after operation	Patient 1		Patient 2		Patient 3	
	Treated side	Normal side	Treated left side	Treated right side	Treated side	Normal side
			(A) Airway D_H (mm)			
Preoperative	1.7 ± 1.3 *n* = 28	3.2 ± 0.4 *n* = 7	2.2 ± 1.0 *n* = 20	4.0 ± 0.6 *n* = 11	1.7 ± 1.3 *n* = 19	4.0 ± 1.2 *n* = 18
1 month	2.5 ± 0.4* *n* = 28	2.9 ± 0.4 *n* = 7	4.8 ± 0.5* *n* = 20	5.4 ± 0.6* *n* = 11	3.6 ± 1.2* *n* = 19	3.7 ± 1.1 *n* = 18
3 months	4.6 ± 0.3 *n* = 17	4.4 ± 0.4 *n* = 9	—	—	4.0 ± 0.1 *n* = 7	4.5 ± 0.4 *n* = 15
6 months	3.8 ± 0.4 *n* = 22	3.6 ± 0.5 *n* = 7	—	—	—	—
12 months	3.5 ± 0.5 *n* = 20	3.9 ± 0.5 *n* = 10	—	—	—	—
30 months	4.0 ± 0.9# *n* = 20	4.5 ± 1.2 *n* = 10	—	—	—	—
			(B) Airway A^2 (mm)			
Preoperative	4.7 ± 4.2 *n* = 28	9.8 ± 2.2 *n* = 7	9.9 ± 8.3 *n* = 20	20.3 ± 2.6 *n* = 11	4.2 ± 4.1 *n* = 19	15.7 ± 6.4 *n* = 9
1 month	6.9 ± 0.8* *n* = 28	8.0 ± 2.1 *n* = 7	21.8 ± 3.1* *n* = 20	30.8 ± 6.0* *n* = 11	13.9 ± 7.0* *n* = 19	14.1 ± 6.4 *n* = 18
3 months	17.5 ± 2.1 *n* = 17	16.5 ± 3.4 *n* = 9	—	—	14.9 ± 1.0 *n* = 7	22.0 ± 5.3 *n* = 15
6 months	12.1 ± 2.9 *n* = 22	11.4 ± 3.2 *n* = 7	—	—	—	—
12 months	10.9 ± 2.4 *n* = 20	11.6 ± 3.9 *n* = 10	—	—	—	—
30 months Postoperative	15.0 ± 6.8# *n* = 20	23.1 ± 11.0 *n* = 10	—	—	—	—

*P < 0.01 versus preoperative. #P < 0.01 versus 1 month, Student's t test (paired, two-sided, α = 0.05).

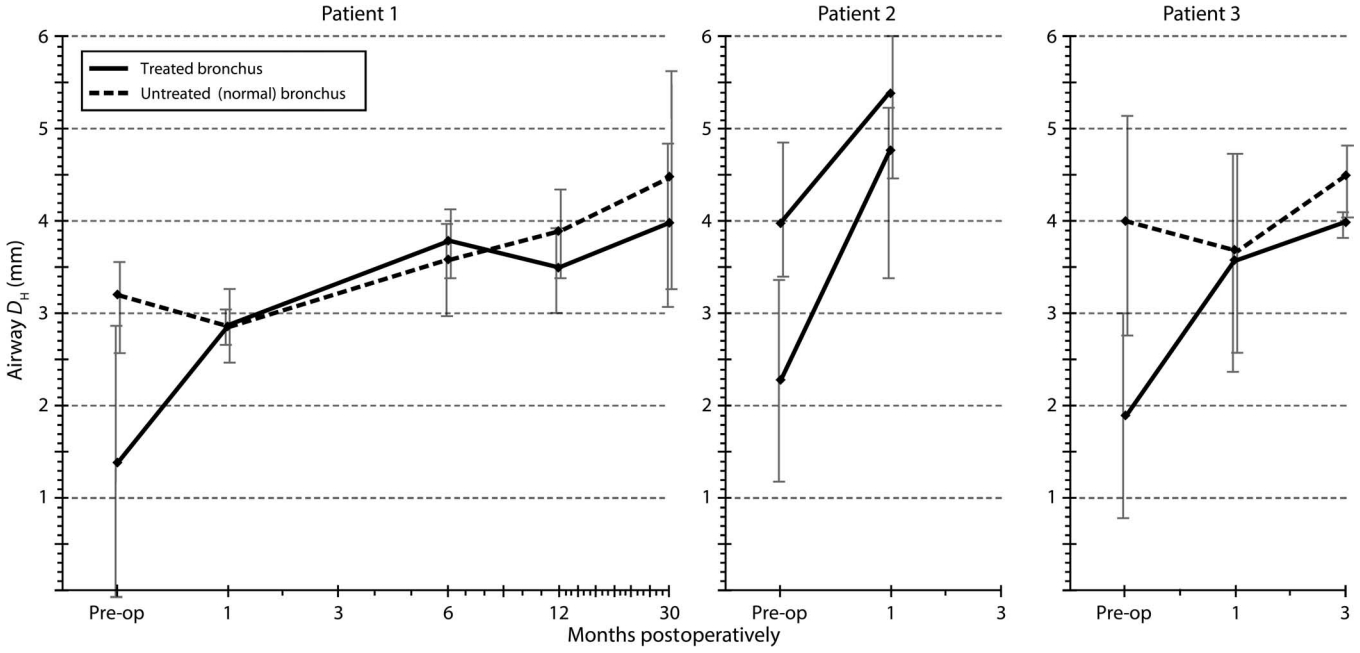

Fig. 4. Mean airway caliber over time. Patient airway D_H was measured over time after implantation of the 3D-printed bioresorbable material. Solid lines denote bronchi that received the tracheobronchial splint. Dashed lines are normal, contralateral bronchi for patients 1 and 3. All caliber measurements were made on expiratory-phase CT imaging using the centerline function of each isolated bronchus in Mimics. The centerline function measures D_H every 0.1 to 1.0 mm along the entire segment of the isolated model. Measurements are represented as averages of all measurements along the length of the isolated affected bronchus model ± SD. Pre-op, preoperative.

pressure (table S2). Patient airway image–based computational design coupled with 3D printing allowed rapid production of these devices. The regulatory approval process and evaluation of patient candidacy needed 7 days. All devices were completed within this time frame. Design and manufacturing could be accomplished within 36 hours if needed.

The potential of 3D-printed medical devices to improve customization and outcomes for patients is clear, but implementation into medical practice faces barriers moving forward. The first 3D devices in medicine have been applied to rare diseases and disorders that do not currently have any acceptable solution. Expanding the use of 3D printing within these niche markets is limited by lack of financial incentives to industry. At present, the regulatory framework for a customizable device intended for rare diseases (<4000 patients per year in the United States) is daunting. Inadequate animal models of human growth also constitute a major barrier in translational studies of 4D biomaterials. Further work will be necessary to characterize the properties of 3D-printed biomaterials and the effect of the 3D printing process on final device performance. Industry guidance is lacking on the proper method to validate materials, manufacturing techniques, sterilization, and performance of 3D-printed devices that vary significantly in form from patient to patient. Fortunately, the FDA is aggressively looking at developing guidance for 3D-printed devices (*34*). The development of improved biomaterials and imaging techniques is needed to increase applicability of this technology (*35*).

Here, we provide a roadmap for 3D printing of 4D biomaterials with FDA-required design control and standard operating procedures to produce implants for treatment of a life-threatening disease. This synthesis of design, material, and manufacturing processes enables patient-specific devices to be produced with time-dependent behavior for growth.

MATERIALS AND METHODS

Study design

Our hypothesis was that an external splint could be designed to obtain sustained airway patency and decrease imminent risk of death in children with life-threatening TBM. All patients were referred from tertiary/quaternary care centers and were confirmed to have intractable immediately life-threatening TBM before transfer via chart and imaging review. All patients were assessed by imaging and operative endoscopy at our institution to confirm the location and severity of TBM. Each patient was individually approved to receive the tracheobronchial splint by the University of Michigan Institutional Review Board and the FDA under the medical device emergency use exemption. An inclusion criterion to receive the tracheobronchial splint was that patients must meet criteria for the FDA emergency use exemption verified by an impartial third-party physician (*36*). Exclusion criteria included responsiveness to other medical or surgical therapies and diffuse severe segmental or subsegmental bronchomalacia. By virtue of the guidelines of the emergency use exemption, investigational devices were restricted to a limited number of uses before the formal regulatory approval process must be pursued, limiting patient recruitment to $n = 3$. This was a prospective, nonrandomized, nonblinded design.

Multidetector CT imaging was used for initial patient evaluation and 3D segmentation of airway anatomy, as well as for postoperative imaging to assess airway caliber. D_H and A^2 were collected at all time points because there is no established method for evaluating airway caliber or growth using patient-specific CAD. Per regulatory guidance, CT imaging of patients was limited to the minimum number necessary to evaluate device safety and as clinically indicated. CT imaging was performed at minimum 1 month postoperatively and then as clinically indicated

on the basis of persistent symptoms of TBM or ongoing ventilatory requirement. MRI imaging was chosen as the modality to assess bioresorption because this was the only modality found that detects the splint in vivo. Annual MRI imaging was planned beginning 1 year postoperatively in all patients.

The time point of 1 month after operation was chosen for assessing effect of the device on airway caliber because minimal tracheobronchial growth is expected in 1 month, minimizing the confounding effect of airway growth from improvement owing to the splint. The 1 and 30-month postoperative time points for patient 1 were chosen for airway growth comparisons. The 1-month postoperative scan eliminated the effect of the splint on airway caliber, and the 30-month postoperative scan provided the furthest time point possible for analysis while the device is undergoing bioresorption. Neither patient 2 nor patient 3 was sufficiently removed from surgery for long-term CT imaging, excluding them from airway growth analysis.

The clinical requirements considered during archetype device design included the following: the splint should provide radial compressive mechanical support, it should provide radial mechanical support for a period of 24 to 30 months, it should allow transverse and bending displacement, it should allow growth of the airway, it should not cause adverse tissue reaction, it should not interfere with mucociliary architecture of the lumen, it should be bioresorbable, and placement should be straightforward.

Device performance parameters and performance testing

Three key identified mechanical performance criteria were identified to ensure appropriate clinical performance of the splint. These include radial mechanical support to maintain airway patency and resist external compressive forces, allowance of transverse bending displacement to allow natural flexion of the airways during respiration, and allowance of displacement of the opening angle of the splint to allow growth and expansion of the tracheobronchial complex. We defined maximum compressive support as <50% deformation under a 20-N load, maximum bending allowance as 20% < x <50% displacement under a 20-N three-point bending load, and minimum opening displacement as >20% under a 15-N load. Rationale supporting these parameters are included in the Supplementary Materials and Methods and are based on previous work (*19*, *37*).

Data collection of peri- and postoperative clinical course, PEEP requirements, albumin levels, and serum immunoglobulin levels was performed by retrospective chart review of patients' perioperative hospitalization at the University of Michigan.

Tracheobronchial splint design, validation, and manufacture

The design parameters for the tracheobronchial splint were input into a proprietary MATLAB (MathWorks) code to generate an output as a series of .TIFF (tagged image file format) image slices using Fourier series representation to generate the waves for bellow structures (Fig. 1D). The .TIFF image files were imported into Mimics and used to generate a surface .STL file of the splint from the image data using a variant of the marching cubes algorithm (Fig. 1A). The splint was then placed over the 3D model of the patient's airway for final design validation (Fig. 1E, fig. S3). Finite element analysis of each splint design was performed to ensure that the design met mechanical performance criteria noted below before manufacture. The verified .STL meshes of the splint designs were used to generate volume meshes with boundary conditions for simulating mechanical testing (Altair HyperMesh, Altair Engineering). Both 8-nodal hexahedral and 10-nodal tetrahedral meshes were generated and tested for convergence.

The splint .STL was subsequently imported into the 3D printer (Formiga P 100 System, EOS e-Manufacturing Solutions) and manufactured via a laser-sintering process from a blend of 96% CAPA 6501 PCL (Polysciences Inc.) and 4% hydroxyapatite (Plasma Biotal Ltd.). PCL was cryogenically milled to a median particle size of 40 to 60 μm (Jet Pulverizer Co.). Hydroxyapatite was used as a flowing agent during the laser sintering process. Printing parameters to laser-sinter PCL are based on previous work by our group and include the following: laser power of 4 W, bed temperature of 50 to 56°C, laser scanning speed of 1000 to 1500 mm/s, and scan spacing of 0.15 to 0.20 mm (*38*–*40*). All splint models were orientated longitudinally along the z axis during slicing. After manufacture, the splints were cleaned via air blasting, followed by sonication in 70% ethanol for 30 min. The splints were peel-packaged and sent to a third party for ethylene oxide sterilization (Nelson Laboratories) at 49.0°C.

Mechanical testing of manufactured splints was performed using an MTS RT/30 Alliance machine. Splint compression testing was performed on the basis of modifications of test parameters defined in FDA guidance on internal vascular stents (*41*). The total deflection under a force of 20 N was measured. Three-point bending was performed to follow American Society for Testing and Materials Standard F2606-08 with the primary exception that the diameter/length ratio of the splint was higher than in stents and the fact that a fixed 20-N load was applied to the specimen and the resulting displacement measured (*42*). Otherwise, the span length and static supports followed F2606. There were no guidance protocols for testing the expansion pressure of a growing trachea or bronchus. Hence, we created a protocol that most closely simulated growth to objectively measure opening percentage of the wedge angle. The splint was positioned within grasping hooks with a resting force of <0.05 N and caliber measurement of <1-mm resting displacement (fig. S4). The testing plates were then separated at a constant rate, and resistance force of the splint was measured. Testing proceeded until device failure.

Patient and device imaging

Imaging of the patient's airway was performed using dynamic multidetector CT. Airway imaging was accomplished using a central airway protocol, which includes thin-cut helical images of the neck and chest in end-inspiratory and dynamic expiratory phase of respiration using intravenous contrast material (slice thickness, 0.625 mm; interval, 0.625 mm; pitch, 1.375:1; kilovolt peak, 80 mA based on body weight; gantry rotation time, 0.5 s full; coverage from 1 cm above epiglottis to base of the lung). Intravenous contrast material was used to delineate adjacent vascular structures. Sagittal and coronal reformatted images as well as MinIP reconstruction and 3D volume rendering of the lungs and airways in both inspiration and expiratory images were performed for further evaluation.

Patient 1 underwent CT imaging at 1, 3, 6, and 12 months postoperatively to establish a radiologic precedent because the patient was the first to receive the splint. Patient 2 underwent CT imaging only at 1 month postoperatively because the patient had no further clinical indications for imaging. Patient 3 underwent CT imaging at 1 and 3 months postoperatively because recovery was slightly prolonged compared to the first two cases. Imaging of the splint to assess bioresorption was performed using MRI, as described in the Supplementary Materials and Methods.

Calculation of airway caliber and growth measurements

DICOM images were imported into Mimics and were used to generate a 3D model of the patient's airway, as described above. A centerline was fit within each bronchus, treated and contralateral, using Mimics. The D_H used for flow calculation of tubes with noncircular diameter and the A^2 were then calculated along the centerline as $D_H = 4A/P$, where A is the cross-sectional area of the bronchi and P is the wetted perimeter of the bronchi. Measurements were calculated by Mimics at 0.1- to 1.0-mm increments along the centerline. Evaluators were not blinded; however, identical procedures were followed for segmentation and measurements in all patient imaging studies.

Statistical analysis

Data are expressed as means ± SD. Statistical analysis was performed with GraphPad Prism software. Statistical analysis of pre- and post-operative PEEP requirements was performed using Mann-Whitney U test given that the data were not normally distributed. Statistical analysis of airway D_H and A^2 measurements was performed using paired two-sided Student's t test. Statistical significance was set to 5% ($\alpha = 0.05$) in all analyses.

SUPPLEMENTARY MATERIALS

www.sciencetranslationalmedicine.org/cgi/content/full/7/285/285ra64/DC1

Materials and Methods

Fig. S1. Contour plot of opening displacement of the tracheobronchial splint under 15-N opening load.

Fig. S2. In vivo placement of tracheobronchial splint.

Fig. S3. Isolation and segmentation of tracheobronchial tree in Mimics.

Fig. S4. Opening displacement testing of the tracheobronchial splint on the MTS RT/30 Alliance machine.

Table S1. Compression, three-point bending, and opening displacement mechanical testing for tracheobronchial splint designs.

Table S2. Predicted changes in tracheal diameter with growth.

Table S3. Venous blood gases before and after splint implantation in patient 1.

Movie S1. Nonlinear finite element analysis demonstration of the tracheobronchial splint response to airway growth.

REFERENCES AND NOTES

1. B. C. Gross, J. L. Erkal, S. Y. Lockwood, C. Chen, D. M. Spence, Evaluation of 3D printing and its potential impact on biotechnology and the chemical sciences. *Anal. Chem.* **86**, 3240–3253 (2014).
2. I. Campbell, D. Bourell, I. Gibson, Additive manufacturing: Rapid prototyping comes of age. *Rapid Prototyp. J.* **18**, 255–258 (2012).
3. G. T. Klein, Y. Lu, M. Y. Wang, 3D printing and neurosurgery—Ready for prime time? *World Neurosurg.* **80**, 233–235 (2013).
4. J. Banks, Adding value in additive manufacturing: Researchers in the United Kingdom and Europe look to 3D printing for customization. *IEEE Pulse* **4**, 22–26 (2013).
5. J. W. Chang, S. A. Park, J. K. Park, J. W. Choi, Y. S. Kim, Y. S. Shin, C. H. Kim, Tissue-engineered tracheal reconstruction using three-dimensionally printed artificial tracheal graft: Preliminary report. *Artif. Organs* **38**, E95–E105 (2014).
6. S. Tibbits, 4D Printing: Multi-Material Shape Change. *Archit. Design* **84**, 116–121 (2014).
7. S. D. Murgu, H. G. Colt, Tracheobronchomalacia and excessive dynamic airway collapse. *Respirology* **11**, 388–406 (2006).
8. R. Boogaard, S.H. Huijsmans, M.W. Pijnenburg, H.A. Tiddens, J.C. de Jongste, P.J. Merkus, Tracheomalacia and bronchomalacia in children: Incidence and patient characteristics. *Chest* **128**, 3391–3397 (2005).
9. V. Goyal, I. B. Masters, B. Chang, Interventions for primary (intrinsic) tracheomalacia in children. *Cochrane Database Syst. Rev.* **10**, CD005304 (2012).
10. M. M. Carr, C. P. Poje, L. Kingston, D. Kielma, C. Heard, Complications in pediatric tracheostomies. *Laryngoscope* **111**, 1925–1928 (2001).
11. J. G. Berry, R. J. Graham, D. W. Roberson, L. Rhein, D. A. Graham, J. Zhou, J. O'Brien, H. Putney, D. A. Goldmann, Patient characteristics associated with in-hospital mortality in children following tracheotomy. *Arch. Dis. Child.* **95**, 703–710 (2010).
12. A. E. Overman, M. Liu, S. C. Kurachek, M. R. Shreve, R. C. Maynard, M. C. Mammel, B. M. Moore, Tracheostomy for infants requiring prolonged mechanical ventilation: 10 Years' experience. *Pediatrics* **131**, e1491–e1496 (2013).
13. E. P. Valerie, A. C. Durrant, V. Forte, P. Wales, P. Chait, P. C. Kim, A decade of using intraluminal tracheal/bronchial stents in the management of tracheomalacia and/or bronchomalacia: Is it better than aortopexy? *J. Pediatr. Surg.* **40**, 904–907 (2005).
14. U.S. Department of Health and Human Services, FDA public health notification: Complications from metallic tracheal stents in patients with benign airway disorders. www.fda.gov/MedicalDevices/Safety/AlertsandNotices/PublicHealthNotifications/ucm062115.htm, issued 29 July 2005 [accessed 2 January 2015].
15. J. B. Haldane, J. M. Smith, in *On Being the Right Size and Other Essays* (Oxford Press, New York, 1985).
16. D. A. Zopf, C. L. Flanagan, M. Wheeler, S. J. Hollister, G. E. Green, Treatment of severe porcine tracheomalacia with a 3-dimensionally printed, bioresorbable, external airway splint. *JAMA Otolaryngol. Head Neck Surg.* **140**, 66–71 (2014).
17. D. A. Zopf, S. J. Hollister, M. E. Nelson, R. G. Ohye, G. E. Green, Bioresorbable airway splint created with a three-dimensional printer. *N. Engl. J. Med.* **368**, 2043–2045 (2013).
18. C. L. Flanagan, W.-J. Tseng, C.-Y. Lin, D. Suárez-González, W. L. Murphy, *et al.*, "In vivo degradation of a novel poly(ε-caprolactone) invertebral cage for anterior cervical discectomy and fusion in a porcine model," paper presented at the Tissue Engineering and Regenerative Medicine International Society (TERMIS) EU Meeting, Galway, Ireland, 13 to 17 June 2010.
19. A. Wright, G. M. Ardran, P. M. Stell, Does tracheostomy in children retard the growth of trachea or larynx? *Clin. Otolaryngol. Allied Sci.* **6**, 91–96 (1981).
20. H. C. Shi, W. J. Deng, C. Pei, D. Lu, X. J. Zhang, X. H. Wang, Y. J. Zeng, Biomechanical properties of adult-excised porcine trachea for tracheal xenotransplantation. *Xenotransplantation* **16**, 181–186 (2009).
21. K. Kida, W. M. Thurlbeck, Tracheal banding in weanling rats diminishes lung growth and alters lung architecture. *Pediatr. Res.* **15**, 269–277 (1981).
22. H. Sun, L. Mei, C. Song, X. Cui, P. Wang, The in vivo degradation, absorption and excretion of PCL-based implant. *Biomaterials* **27**, 1735–1740 (2006).
23. T. L. Gerstle, A. M. Ibrahim, P. S. Kim, B. T. Lee, S. J. Lin, A plastic surgery application in evolution: Three-dimensional printing. *Plast. Reconstr. Surg.* **133**, 446–451 (2014).
24. C. Schubert, M. C. van Langeveld, L. A. Donoso, Innovations in 3D printing: A 3D overview from optics to organs. *Br. J. Ophthalmol.* **98**, 159–161 (2014).
25. J. A. Gillis, S. F. Morris, Three-dimensional printing of perforator vascular anatomy. *Plast. Reconstr. Surg.* **133**, 80e–82e (2014).
26. I. D. Ursan, L. Chiu, A. Pierce, Three-dimensional drug printing: A structured review. *J. Am. Pharm. Assoc.* **53**, 136–144 (2013).
27. K. Wren, Science and society. Experts warn against bans on 3D printing. *Science* **342**, 439 (2013).
28. K. B. Chien, E. Makridakis, R. N. Shah, Three-dimensional printing of soy protein scaffolds for tissue regeneration. *Tissue Eng. Part C Methods* **19**, 417–426 (2013).
29. R. Partridge, N. Conlisk, J. A. Davies, In-lab three-dimensional printing: An inexpensive tool for experimentation and visualization for the field of organogenesis. *Organogenesis* **8**, 22–27 (2012).
30. F. Rengier, A. Mehndiratta, H. von Tengg-Kobligk, C. M. Zechmann, R. Unterhinninghofen, H. U. Kauczor, F. L. Giesel, 3D printing based on imaging data: Review of medical applications. *Int. J. Comput. Assist. Radiol. Surg.* **5**, 335–341 (2010).
31. P. Bugmann, P. C. Rimensberger, A. Kalangos, C. Barazzone, M. Beghetti, F. J. Lang, Extratracheal biodegradable splint to treat life-threatening tracheomalacia. *Ann. Thorac. Surg.* **78**, 1446–1448 (2004).
32. J. H. Cho, H. Kim, J. Kim, External tracheal stabilization technique for acquired tracheomalacia using a tailored silicone tube. *Ann. Thorac. Surg.* **94**, 1356–1358 (2012).
33. T. Sakamoto, Y. Nagase, H. Hasegawa, T. Shin'oka, H. Tomimatsu, H. Kurosawa, One-stage intracardiac repair in combination with external stenting of the trachea and right bronchus for tetralogy of Fallot with an absent pulmonary valve and tracheobronchomalacia. *J. Thorac. Cardiovasc. Surg.* **130**, 1717–1718 (2005).
34. U.S. Department of Health and Human Services, Additive manufacturing of medical devices: An interactive discussion on the technical considerations of 3D printing; public workshop. www.fda.gov/MedicalDevices/NewsEvents/WorkshopsConferences/ucm397324.htm. 8 to 9 October 2014.
35. S. V. Murphy, A. Atala, 3D Bioprinting of tissues and organs. *Nat. Biotechnol.* **32**, 773–785 (2014).
36. Investigational Device Exemptions, Code of Federal Regulations, title 21, vol. 8, part 812, subpart B, Section 812.36, revised 1 April 2014 [accessed 30 October 2014].
37. S. J. Hollister, C. L. Flanagan, D. A. Zopf, R. J. Morrison, H. Nasser, J. J. Patel, E. Ebramzadeh, S. N. Sangiorgio, M. B. Wheeler, G. E. Green, Design control for clinical translation of 3D printed modular scaffolds. *Ann. Biomed. Eng.* **43**, 774–786 (2015).

38. J. M. Williams, A. Adewunmi, R. M. Schek, C. L. Flanagan, P. H. Krebsbach, S. E. Feinberg, S. J. Hollister, S. Das, Bone tissue engineering using polycaprolactone scaffolds fabricated via selective laser sintering. *Biomaterials* **26**, 4817–4827 (2005).
39. B. Partee, S. J. Hollister, S. Das, Selective laser sintering process optimization for layered manufacturing of CAPA 6501 polycaprolactone bone tissue engineering scaffolds. *J. Manuf. Sci. Eng.* **128**, 531–540 (2006).
40. M. H. Smith, C. L. Flanagan, J. M. Kemppainen, J. A. Sack, H. Chung, S. Das, S. J. Hollister, S. E. Feinberg, Computed tomography-based tissue-engineered scaffolds in craniomaxillofacial surgery. *Int. J. Med. Robot.* **3**, 207–216 (2007).
41. U.S. Department of Health and Human Services, Guidance for industry and Food and Drug Administration staff: Non-clinical engineering tests and recommended labeling for intravasular stents and associated delivery systems, www.fda.gov/downloads/MedicalDevices/DeviceRegulationandGuidance/GuidanceDocuments/ucm071986.pdf, issued 18 April 2010 [accessed 1 October 2014].
42. ASTM Standard F2606-08, Standard guide for three-point bending of balloon expandable vascular stents and stent systems (ASTM International, West Conshohocken, PA, 2014).

Acknowledgments: We thank C. Flanagan for help with splint design vetting, manufacturing, and processing; H. Nasser for help with splint processing and testing; K. Khanafer for help with contact finite element analysis; and the Michigan Institute for Clinical and Health Research IND (Investigational New Drug)/IDE (Investigational Device Exemption) Investigator Assistance Program. **Funding:** This work was funded in part by NIH grant R21 HD076370-01 (to S.J.H. and G.E.G.). Device development was funded by NIH grant UL1 RR024986 and FDA grant P50 FD003787. R.J.M. is supported by NIH grant T32 DC005356-12. **Author contributions:** R.J.M. was involved in device design and manufacture, collected and analyzed data, and wrote the paper. S.J.H. and G.E.G. are co-inventors of the device and were involved in device design and data analysis. M.F.N. was involved in postoperative care of study subjects and data analysis. M.G.M. was involved in developing the radiologic protocols to image the patients, provided guidance for developing the methods of the study, and was involved in the postoperative care of the patients. A.H.P. and D.K.M. were equally involved in the pre- and postoperative care of study subjects. R.G.O. was involved in implantation of the device and postoperative care of study subjects. All authors discussed the results and commented on the manuscript. **Competing interests:** S.J.H. and G.E.G. have filed a patent application related to the device. The authors declare no other competing financial interests. **Data and materials availability:** All data and materials are available upon request. The MATLAB code used to generate the tracheobronchial splint design is proprietary; however, we are willing to design a device from our code for those interested.

Submitted 2 October 2014
Accepted 23 February 2015
Published 29 April 2015
10.1126/scitranslmed.3010825

Citation: R. J. Morrison, S. J. Hollister, M. F. Niedner, M. G. Mahani, A. H. Park, D. K. Mehta, R. G. Ohye, G. E. Green, Mitigation of tracheobronchomalacia with 3D-printed personalized medical devices in pediatric patients. *Sci. Transl. Med.* **7**, 285ra64 (2015).

Science Translational Medicine
AAAS

Mitigation of tracheobronchomalacia with 3D-printed personalized medical devices in pediatric patients

Robert J. Morrison *et al.*

Sci Transl Med **7**, 285ra64 (2015);
DOI: 10.1126/scitranslmed.3010825

Editor's Summary

Printing in 4D: Personalized implants

The 3D printing revolution is in full swing, with frequent reports of printed kidneys and jaws, dolls and cars, food, and body armor. The new challenge is to make 3D materials evolve in the fourth dimension: time. Such "4D" materials could change in response to temperature, light, or even stress, making them adaptable and enduring. In pediatric medicine, 4D implants become particularly relevant; as the patient grows, so, too, should the material. Morrison *et al.* used 3D printing technology with a safe, bioresorbable polymer blend to create splints for three pediatric patients with tracheobronchomalacia (TBM) ––a condition of excessive collapse of the airways during normal breathing. Currently available fixed-size implants can migrate and require frequent resizing. Thus, the authors used imaging and computational models to design the splints for each TBM patient's individual geometries, structuring the implants to accommodate airway growth and prevent external compression over a period of time, before being resorbed by the body. In all three patients (one with two airways splinted), the 4D devices were implanted without issue. All four implants were stable and functional after 1 month, and one implant has remained in place, keeping the airway open for over 3 years. This pilot trial demonstrates that the fourth dimension is a reality for 3D-printed materials, and with continued human studies, 4D biomaterials promise to change the way we envision the next generation of regenerative medicine.

Science Translational Medicine (print ISSN 1946-6234; online ISSN 1946-6242) is published weekly, except the last week in December, by the American Association for the Advancement of Science, 1200 New York Avenue NW, Washington, DC 20005.